A Computational Study Of Heat Transfer Due To The Inlet Oscillating Conditions In A 2-D Jet Impinging On An Isothermal Surface At A Fixed Reynolds Number

Issa[1], J., Saliba[2], N., Sidnawi[3], B.

[1]Department of Mechanical Engineering, University of Balamand, El koura, Lebanon
[2]Department of Civil Engineering, University of Balamand, El koura, Lebanon
[3]Department of Mechanical Engineering, Villanova University, PA 19085, USA

--**ABSTRACT**--

Heat transferis numerically investigated in aconfined oscillating laminar slot jet. The inlet velocity profile is uniform, and oscillating with an angle φ (in radians) as follows:$\varphi = \varphi_{max} * sin(2\pi f t)$.$\varphi_{max}$ is the maximum jet angle, and f is the frequency of oscillation. The height-to-jet-width ratio was set to 5, the fluid's Prandtl number is 0.74 and Reynolds number was fixed at 250.Strouhal's numberSt, which is the other dimensionless group characterizing this problem, was varied in the range 0.05<St<0.75.The jet hydraulic diameter (2w), was used in the definition of both Strouhal and Reynolds numbers. φ_{max} was defined, based on a solid finding presented later in this paper. At St=0.4, and 0.5, a modest enhancement of heat transfer was noticed in the stagnation region, when compared to a steady jet.

Keywords:oscillating jet, heat transfer

I.   INTRODUCTION

Fluid jets proved to be very useful in several industrial applications, such as drying, cooling of a heated surface, aerodynamic control and flow separation control. Electronic circuits are getting smaller and faster, which increases the density of heat dissipation and gives rise to the need for new cooling technologies. Impinging jets seem to be a promising technology that could catch up with the advancements of the electronics industry.

In the numerical study conducted by Ebrahim et al. [1], it shown that a circular sinusoidal synthetic jet impinging on a heated surface, could enhance the overall heat transfer compared to the steady jets having a higher stagnation Nusselt number. The overall Nusselt number averaged over both space and time appeared to be depending on Reynolds number and the jet-to-wall distance. As the frequency is increased, the space averaged Nusselt number increased. However the stagnation Nusselt number decreased due to the non-linear merging of vortices. When the frequency was excessive heat transfer was decreased. The enhancement shown in this study [1] was due to the generated vortex rings hitting, then crawling the surface.

In a numerical study by Marzouk et al. [2] on free and wall pulsed two-dimensional laminar plane jets, a sinusoidal pulsation was applied to the flow out of the jet. For the free jet, the study showed that the pulsation only affects the flow in the vicinity of the nozzle, which is revealed by an accelerated development and entrainment of the flow. For the wall jet, both adiabatic and isothermal walls were considered. It was also noticed that the periodic nature of the flow would persist for longer distances downstream of the jet for lower Strouhal numbers, which was interpreted by the increasing intensity of the puffs for lower frequencies. At a Strouhal number of 0.3, increasing the amplitude (A) increased the heat transfer at the wall. When the Strouhal number exceeded 0.6 it had no more influence on heat transfer and the enhancement of the averaged Nusselt number was of about 9% for all considered Strouhal numbers.

Another computational study by HeeJoo et al. [3], showed interesting flow features in semi-confined axi-symmetric pulsed laminar impinging water jets. The used pulsation was sinusoidal. It was found that at the radial position where the Nusselt number maintained a constant value during one oscillation cycle, the flow separates in the wall jet region. This was interpreted as being the effect of vortices above that location, which hindered the deceleration and acceleration of the flow during every cycle. The best heat transfer performance was found at *Re* = 300, at a frequency of 5 Hz and a height-to-width ratio of 9.

Kim [4] numerically investigated heat transfer in a pulsed laminar slot jet impinging on a surface for Reynolds number values of 50 and 150. The velocity of the expelled fluid from the jet is uniform, and it is of a square wave form as a function of time with a 100% modulation (amplitude) about the average, and a duty cycle of 50%. The Strouhal number was varied. At *St* = 0.5, the stagnation Nusselt number improved by almost 23%

compared to the steady case. Compared to the case where *St* = 0.5, at 0.05 the vortex pair is so large that it manages to interact with the next one, which interferes with the latter's ability to remove heat.

The jet stability problem was tackled by Chiriac et al. [5] in the study that investigated the flow behavior, as well as the heat transfer in a confined slot jet impinging on an isothermal surface. The height-to-jet-width ratio fixed to 5, and Reynolds number was the only variable. The flow presented a steady behavior up to a Reynolds number somewhere between 585 and 610. At 250 the flow separates from the target wall at a position close to the stagnation point, because of the low momentum that could not overcome the re-entrainment effect due to the jet. As Reynolds number increased, the separation location was going further from the stagnation region. At 750 the flow presented an unsteady flapping behavior. This was strongly related to the confinement effect. The average Nusselt number distribution was the highest, and even higher than a hypothetical steady counterpart, because non-linear effects made the dependency of heat transfer on Reynolds number a minor one.

In an experimental study carried out by Camci et al. [6], on self-oscillating impinging jets for three high Reynoldsnumbers, 7500, 10000, and 14000, and a jet-to-surface distance ranging from 24 to 60 jet diameters, it was shown that the flapping motion significantly enhanced thermal transport near the impingement plate. The oscillation also increased convection and diffusion. The enhancement zone of heat transfer on the impingement surface due to oscillation, was widened significantly, when compared with a stationary jet. For the Reynolds numbers and jet to surface distances mentioned above, the enhancement of the heat transfer coefficient ranged from 20% to 70% over the stationary jets.

In the present numerical study, heat transfer in a forced oscillating impinging jet at H/w = 5, for *Re* = 250 belonging to the self-stable range established by Chiriac et al. [5], is investigated. The inlet velocity vector had a constant magnitude, and based on which *Re* was defined, and its direction is oscillating in a prescribed sinusoidal shape for various dimensionless frequencies ranging from 0.05 to 0.75. The commercial CFD code FLUENT was used to solve this problem. The heat transfer enhancement found by Chiriac et al. [5] which was due to flapping, was the motivation behind this study.Therefore, it was deemed worthy trying to engage the jet into flapping by means of the oscillating inlet conditions, and see if the response of heat transfer would exhibit any similar enhancement.

II.   PROBLEM DESCRIPTION

2.1 Computational domain

In this problem, a two-dimensional oscillating slot jet impinging on an isothermal surface is investigated, with air as the working fluid. Strouhalnumbers (*St*) considered, ranged from 0.05 to 0.75, and the considered Reynolds number is *Re* = 250. A Cartesian coordinate system is used in the rectangular computational domain shown in Fig. 1 below. The origin coincides with the inlet's center. The positive x direction is to the right, and the positive y direction is downward. The assumed constant values of air properties were as follows:

$$\rho = 1.1184 \text{ kg/m}^3, C_p = 1006.43 \text{ J/kg.K}, k = 0.0242 \text{ W/m.K}, \mu = 1.7894*10^{-5} \text{ kg/m.s}$$
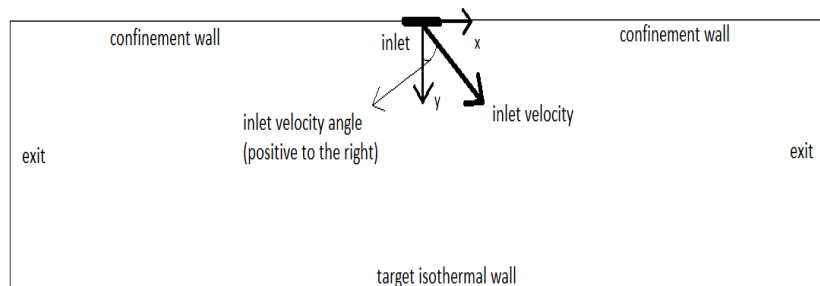

Fig. 1. A sketch describing the current problem

1.2   Governing Equations and Boundary Conditions

The two-dimensional flow in the channel is assumed to be laminar, unsteady, and incompressible. In the energy equation, kinetic dissipation terms are neglected. Hence, the equations governing the flow are:

$$\nabla.\vec{V} = 0 \qquad (1)$$

$$\frac{D\vec{V}}{Dt} = -\frac{\nabla P}{\rho} + \nu\nabla^2\vec{V} \qquad (2)$$

$$\frac{DT}{Dt} = \alpha\nabla^2 T \qquad (3)$$

The target wall is isothermal, and the upper wall is adiabatic, with assumed no-slip and impermeable conditions for both walls. The boundary conditions for which equations (1), (2), and (3) were solved, are:

➢ -12.5w < x < -0.5w and 0.5w < x < 12.5w, y = 0 (At the confinement wall):

$$u = v = 0$$

$\frac{\partial T}{\partial y} = 0.$

➢ -12.5w < x < 12.5w, y/w = H/w = 5(At the target wall):

$$u = v = 0$$

$T = T_w = 310$ K.

➢ x/w = -12.5, and x/w = 12.5 (A zero gradient for all quantities at the exits):

$$\frac{\partial u}{\partial x} = \frac{\partial v}{\partial x} = \frac{\partial T}{\partial x} = 0$$

➢ inlet -0.5w < x < 0.5w, y = 0 (An oscillating velocity profile at the):

$$V_{inlet} = constant$$
$$\varphi = \varphi_{max} * \sin(2\pi f t)$$

$T = T_0 = 300$ K.

Hence, at the inlet:

$$u = V_{inlet} \sin(\varphi)$$
$$v = V_{inlet} \cos(\varphi)$$

➢ As for the initial conditions, the flow was initiated at t = 0 as follows:

$T = T_0 = 300$ K, u = v = 0, everywhere.

φ_{max} was established based on the *Nu* distributions for the steady cases corresponding to *Re* = 100, 250, and 400. The results are summarized in Fig. 2 below.
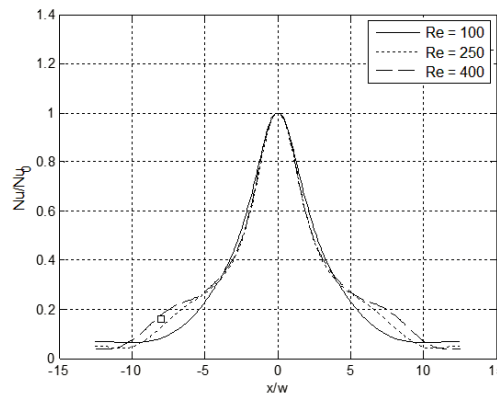

Fig. 2. The normalized *Nu* distribution for the three corresponding steady cases

The average of each distribution, between the two span-wise locations where it starts becoming flat, was taken. Subsequently, the two span-wise locations (± x_0/w) where that average value occurred, was considered. The results are shown below:

Re = 100, x_0/w = 3.3.
Re = 250, x_0/w= 3.9.
Re = 400, x_0/w = 3.8.

The three values of x_0/w had an average of 3.67, from which the value for *Re* = 100 departs by a maximum of 10%. Based on this, the angle from the y-axis intercepting the location x/w = 3.67 at the wall, was defined as φ_{max}. Hence:

$$\varphi_{max} = tan^{-1}\left(\frac{3.67}{5}\right) = 0.633\ rad = 36.28^o$$

Interestingly, that average value of x/w is the exact same value at which the three curves intersect as shown in Fig. 2 above (those of $Re = 250$, and 400, being almost overlapping for $|x/w| < 5$). Since the way φ_{max} was defined, is based on a feature that characterizes a fair span of the self-stable Re range established by Chiriac et al. [5], it was considered to be a solid definition.

1.3 Numerical solution

The finite volume CFD code FLUENT was utilized to solve this problem. After a space and time grid independence study, and taking the computational time along with the convergence behavior into account, it was found that a structured 250x120 mesh was sufficiently fine grid, with a time step of 0.1ms where the transient formulation was first order implicit. The cells had to be refined near the walls in order to capture the high gradients. The SIMPLE scheme was used for the pressure-velocity coupling, and the convective terms in the momentum and energy equations were discretized using the second order upwind scheme.

The convergence was declared at 10^{-6} scaled residuals for the momentum and continuity equations, and 10^{-8} for the energy equation.
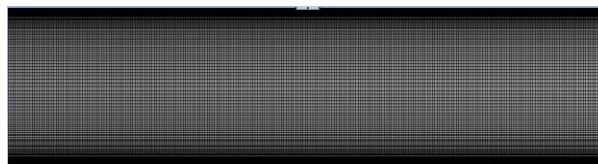

Fig. 3. The mesh used to solve this problem

The flow time simulated for most of the cases was 6s. The dimensionless computational time ranged from 6 to 144 oscillations. With the available equipment, each simulation took about 5 days to finish, which is relatively expensive. Therefore, time constraints did not allow longer simulations.

III.   BENCHMARKING PROBLEM

Before carrying out any simulation in the present study, and to be confident about the used commercial CFD code, the case of $Re = 250$ considered in [5] was computed again using the code just mentioned. The same boundary conditions as those of the current problem (also identical to those used in [5]), were used with a constant downward velocity at the inlet. The same grid shown in Fig. 3 above, along with the pressure-velocity coupling and discretization schemes mentioned in Sect. 2.3 were used. Since in the study of Chiriac et al. [5] it was shown that a Reynolds number of 250 belongs to the self-stable range, it was defensibly reasonable to model the flow as steady. The results comparison is shown in Fig. 4 below.
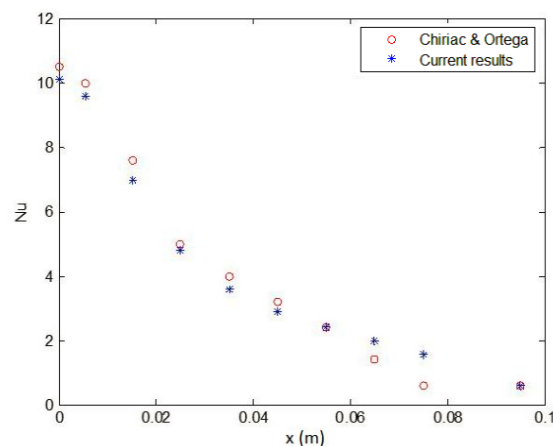

Fig. 4. Comparison of the *Nu* distribution to the one obtained by Chiriac and Ortega

Only one side of the channel was taken for comparison, since both data sets were symmetric about the y-axis. There was an almost perfect agreement at x = 0.055 m, and 0.095 m. Beside the different discretization schemes used for the convective terms in the energy and momentum equations (in [5] the QUICK scheme was used), the difference in the results is mainly attributed to the difference between the grids. The grid used in the original study is an 84x62 grid, in contrast to the grid shown in Fig. 3, yet the refined 250x120 grid seemed necessary, since for the currently treated problem, it gave the best convergence behavior.

As an overall assessment, the plots were entangled smoothly enough for them to compare well. In this section, it was established that published results could be fairly attained, using the ANSYS FLUENT commercial code.

IV.   RESULTS AND DISCUSSIONS

For *Re* = 250, eight frequencies were studied. In dimensionless form, these are: *St* = 0.05, 0.1, 0.2, 0.3, 0.4, 0.5, 0.6, and 0.75; respectively corresponding to the dimensional frequencies:1Hz, 2 Hz, 4 Hz, 6 Hz, 8 Hz, 10 Hz, 12 Hz, and 15 Hz.

The lowest tow frequencies, *St* = 0.05, and 0.1, resulted in flow fields that would be considered counter intuitive; because of the obvious asymmetry. As shown in the velocity contours of Fig. 5 below, both flows were more developed to the right side of the channel.

St=0.05, after 6 oscillations

St=0.1, after 12 oscillations
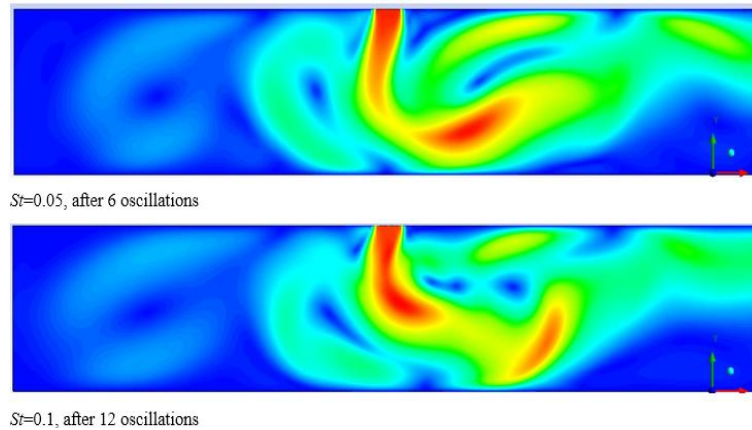
Fig. 5. Snapshots of the velocity distributions for *St* = 0.05, and 0.1

The underlying cause for this behavior resides in the entraining effect induced by the first swing of the jet which is to the right. At these low frequencies, the first swing has enough time to entrain the nearby fluid to the right. This entrained fluid will have developed enough to make it harder for the next swing that is to the left, to restore balance. This breaks the symmetry, since the third swing will be to the right side which already has a more developed flow. Hence, an amplification of this imbalance will occur during every oscillation period; which explains the developed right side flow fields shown above. It might be suspected that the flow fields will eventually become symmetric if given enough time. But the persistence of this flow pattern even when the frequency is doubled, allowing only half the time for the first right swing to initiate a flow to a preferable side, and giving a double amount of left swings to compensate for the imbalance; makes this suspicion unlikely. As demonstrated later, this effect will eventually disappear, for greater values of *St*.

As shown in Fig. 6 below, a similar asymmetry for the *Nu* distribution over the wall should be expected, since heat transfer is a strong function of the flow field. The instantaneous Nusselt number distributions were averaged over the last 2 periods for *St* = 0.05, and the last period for *St* = 0.1, in order to obtain the distributions shown below.
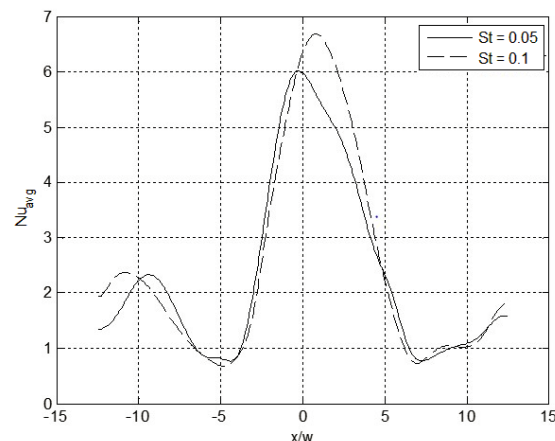

Fig. 6. The average *Nu* distributions for *St* = 0.05, and 0.1

It can be seen that the maximum *Nu* is greater for *St* = 0.1. This may be interpreted by the more intense vortical motion induced by the higher frequency. Due to the vortices above the location x/w = -10 for both frequencies (shown in Fig. 5), one also notices a significant local peak near that location, which is in agreement with the findings of Ebrahim et al. [1].

4.1 St = 0.2 (f = 4Hz)

For *St* = 0.2, asymmetry was considerably reduced but still present. At this frequency, the oscillations produced well-structured vortices that crawled on the wall for a certain distance, after hitting it; causing a local peak propagation in the instantaneous wall *Nu* distribution. After tf = 20 (tf is the number of jet oscillations as the dimensionless time), the propagation becomes apparent. This is shown in Fig. 7 below. Vorticity is defined as the curl (circulation density) of the velocity field. Formally:

$$\vec{\omega} = \vec{\nabla} \times \vec{V}$$

Which in this two dimensional case becomes:

$$\omega = \frac{\partial v}{\partial x} - \frac{\partial u}{\partial y}$$
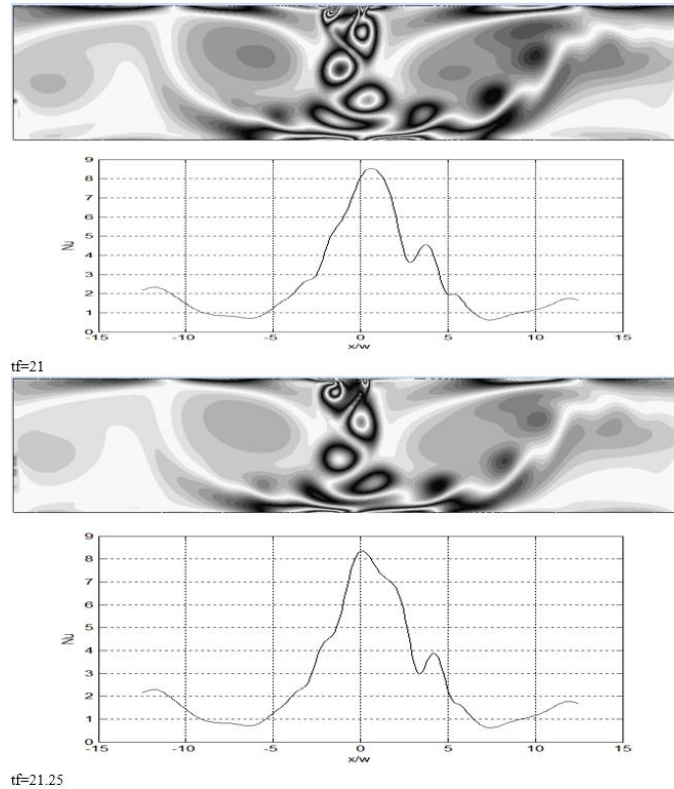
Fig. 7. Instantaneous *Nu*, and corresponding vorticity distributions at tf = 21, and 21.25

As shown in the Fig. 7 above, there are 2 local peaks that can be traced along with each one's corresponding vortex. Since the frequency is still low, the effect discussed for *St* = 0.05 and 0.1 is still present. The propagation shown keeps that same pattern until t = 6s, which is 24 oscillations. Therefore, the averaged sample instants where from tf = 21 to tf = 24.

Due to the recirculating region on the far left, which has a better structure than the one on the right, a slightly higher *Nu* was present on the wall beneath it; as shown in Fig. 8 below.
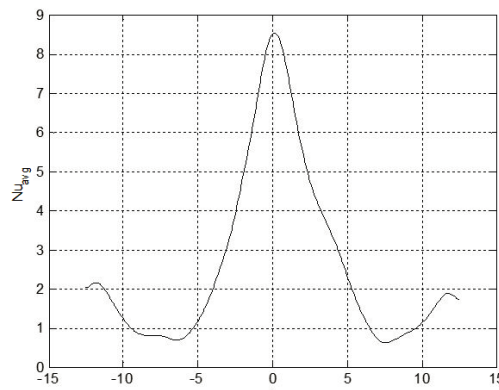

Fig. 8. The average Nu distribution for St = 0.2

It becomes more evident that vortical motion has a major role in enhancing heat transfer. The squeezing effect that the present local vortices have on the thermal diffusive layer is obvious in Fig. 9 below; making it thinner and hence increasing the temperature gradient at the wall.
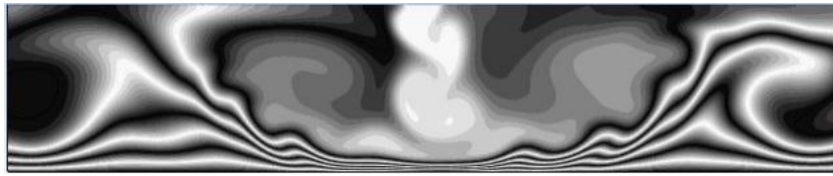

Fig. 9. Instantaneous temperature contours at tf = 24

4.2 St = 0.3 (f = 6Hz)

When *St* was increased to 0.3, asymmetry was further reduced and the vortices became harder to trace after hitting the wall, making the propagating peaks dimmer. Fig 10 below, shows a few snapshots of instantaneous *Nu* distributions.
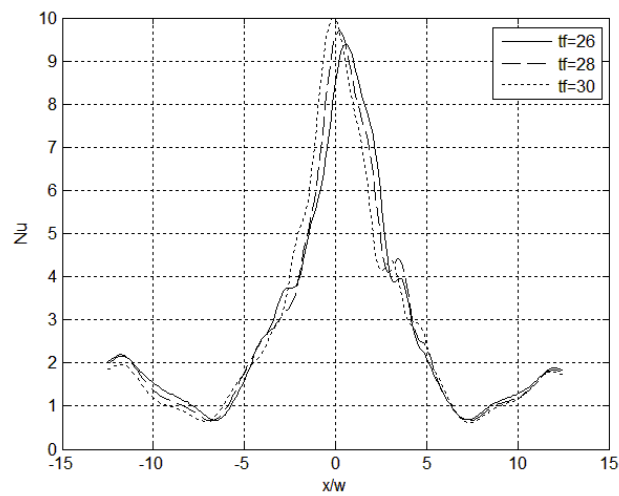
Fig. 10.*Nu* evolution from tf = 26 to tf = 30

Due to the shorter period, the jet has less time to roll up a vortex that is strong enough to withstand longer distances. However, with a greater frequency the bulk flow heading toward the wall can build up a greater momentum, which contributes to a greater Nu_0. ThisisshowninFig. 11 below.
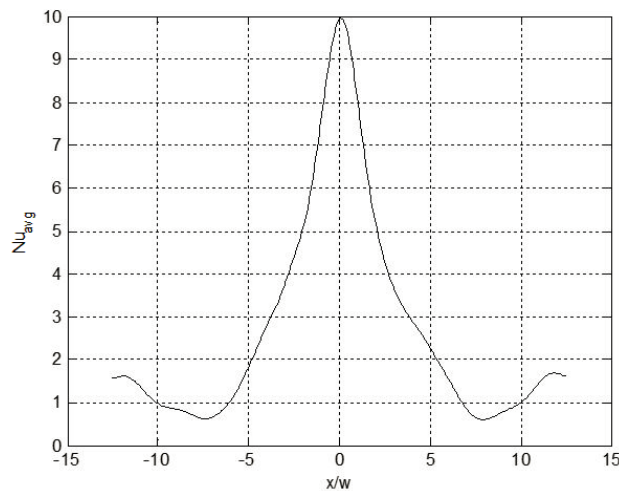

Fig. 11. The average *Nu* distribution for *St* = 0.3

The squeezing effect discussed earlier, is less apparent for *St* = 0.3 and this is due to the dimmer vortices. In Fig. 12 below, the thinner diffusive layer in the stagnation region indicates a higher temperature gradient, hence the higher Nu_0 than that of *St* = 0.2.
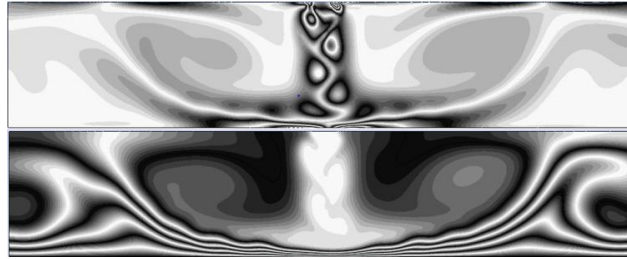
Fig. 12. Instantaneous vorticity (upper) and temperature (lower) contours at tf = 35.5

As a part of the flow seeks its way between the inner and outer recirculation, the span-wise velocity decreases which weakens convective heat transfer. Hence, the thicker diffusive layer at about |x/w| = 7.5.

4.3 St = 0.4 (f = 8Hz)

At St = 0.4, the vortices almost vanished at the instant they hit the wall. The Nusselt number distribution was even more symmetric and interestingly, Nu_0 was higher than that of the steady case, though not substantially. The Nusselt number evolution is shown in Fig. 13 below.
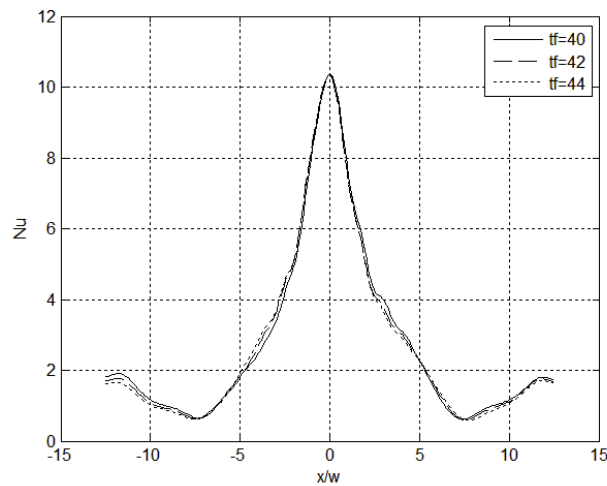

Fig. 13. Nu evolution from tf = 40 to tf = 44

As of tf = 44, the Nu_0 position is set in a subtle back and forth motion about x/w = 0, which continues in the same way until tf = 48. The time averaged Nusslet number is shown in Fig. 14.
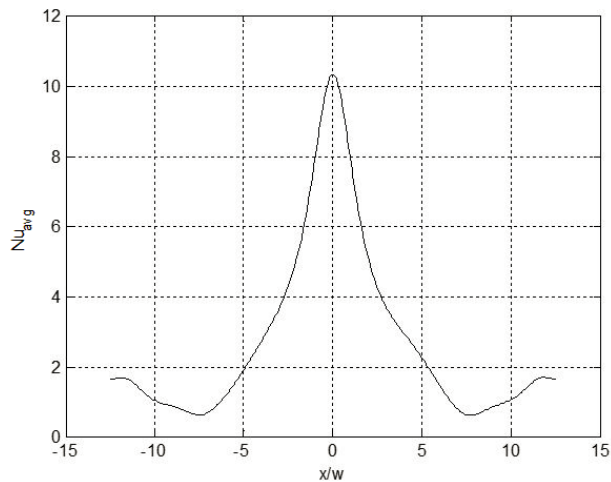

Fig. 14. The average wall Nu distribution for St = 0.4

Nu_{avg} distribution shows an almost completely recovered symmetry, except around |x/w| = 5. The effects of recirculation on the far left and right sides are still present. St = 0.4 and 0.5 belong to a critical range, as shall be concluded later. This is because both values of St present a Nu_0, even higher than the stagnation Nu_0 of the

steady state case. It seems like at these values of Strouhal number, the combination of high bulk momentum and vortical motion is constructive.

Due to the nearly decayed vortices, as observed for instantaneous *Nu* distributions, this layer is very lightly squeezed at locations corresponding to |x/w<5. As shown in Fig. 14 below, the recirculating regions at about |x/w| = 12 are still leading to a thinner diffusive layer, presenting local peaks in Nu_{avg} at those two locations.
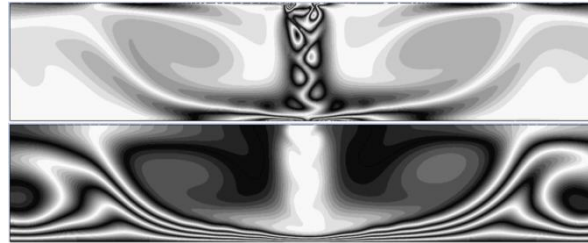

Fig. 15. The instantaneous vorticity and temperature contours at tf = 48

4.4 St = 0.5 (f = 10Hz)
The results corresponding to *St* = 0.5 were very similar to those of *St* = 0.4. The average *Nu* distribution is shown in Fig. 16 below.
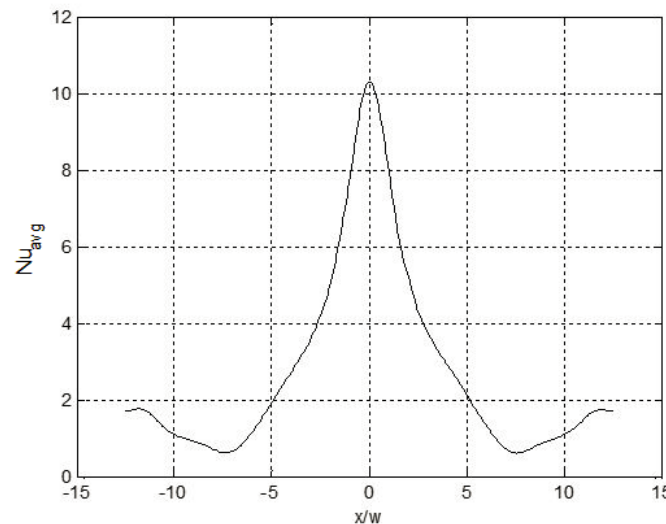

Fig. 16. The average wall *Nu* distribution for *St* = 0.5

Compared to the case of *St* = 0.4, symmetry is improved at |x/w| = 5. As shown in Fig. 17 below, the diffusive layer is thin at the stagnation and the vortical effect is completely absent; as if the jet were steady. The recirculating regions are still making the diffusive layer thinner at |x/w| = 12, causing Nu_{avg} to peak.
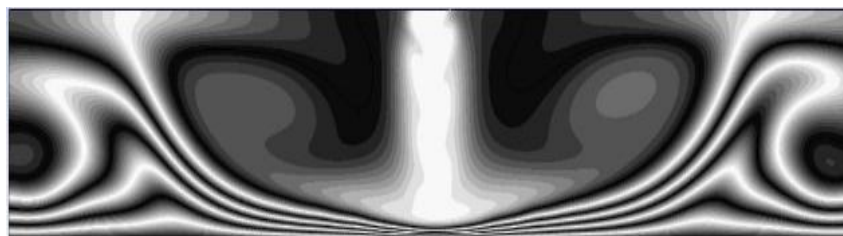

Fig. 17. Temperature contours at tf = 60

4.5 St = 0.6 (f = 12Hz)
When the frequency was further increased to *St* = 0.6, Nu_0 decreased back to a value that is still a bit higher than the steady Nu_0 (Fig. 18 below). At this frequency, the vortices were so weak that they could barely reach the wall. This is linked to a finding by Marzouk et al. [2], about the decreasing downstream distance; up to which pulsing effects can reach, as the pulsation frequency increases for the same amplitude. It is as if these effects were almost cancelled out by the higher bulk momentum reaching the wall, if the steady state is taken as a reference. In Fig. 19 below, one can see the weakness of the vortices as they touch the wall.
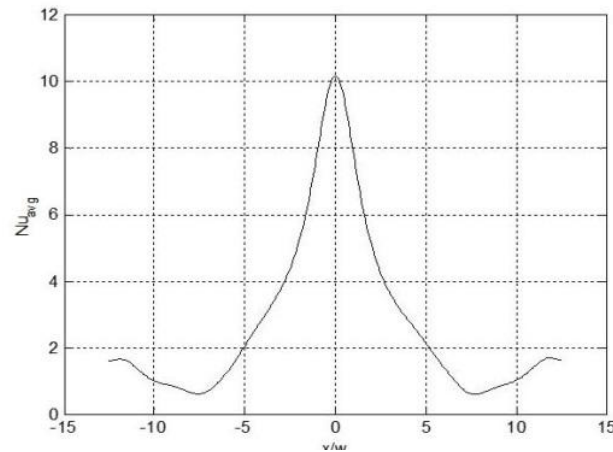
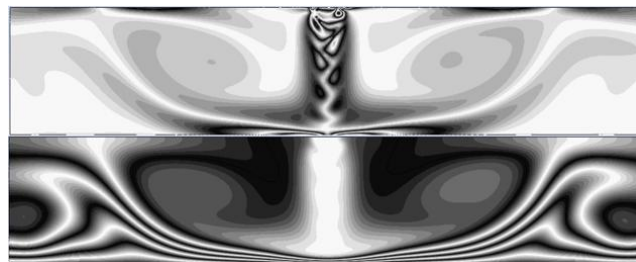**Fig. 18.** *Nu* average distribution for *St* = 0.6 (almost perfect symmetry)

Fig. 19. The instantaneous vorticity and temperature contours at tf = 69.6

4.6 St = 0.75 (f = 15Hz)

At *St* = 0.75, Nu_0 went back to a lower value than the one corresponding to the steady case. As shown in Fig. 21 below, generated vortices were even weaker and did not reach the wall; on top of which, the bulk momentum was too much compromised to compensate. Which could explain the lower average Nu_0 shown in Fig. 20 below.
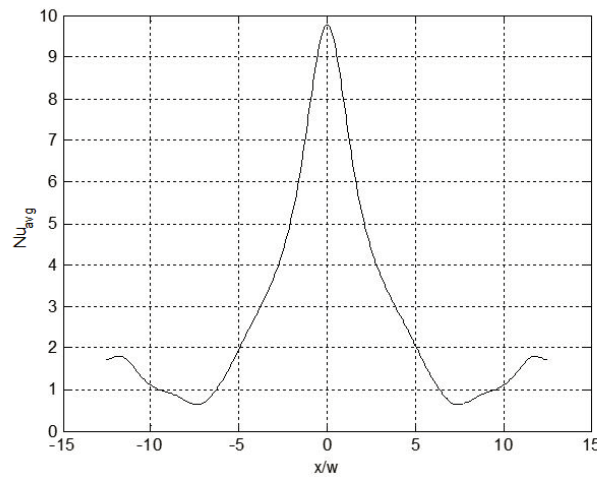

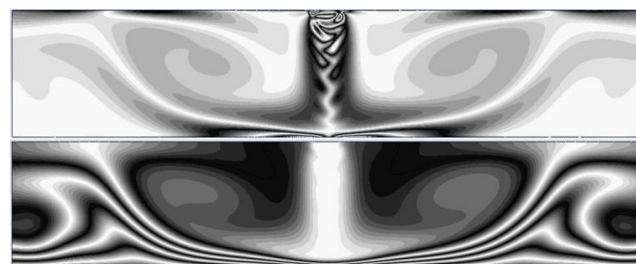**Fig. 20.** Average *Nu* distribution for *St* = 0.75 (symmetry completely recovered)

Fig. 21. The instantaneous vorticity and temperature contours at tf = 90

V. CONCLUSION

This numerical study investigated the heat transfer in a laminar oscillating confined slot jet, impinging on an isothermal surface; at a Reynolds number of 250 belonging to the self-stable range, established by the numerical study of Chiriac et al. [5]. The imposed oscillation at the inlet was sinusoidal. The Strouhal number values that were investigated, ranged from $St = 0.05$ to 0.75. The channel height-to-jet-width ratio was fixed to 5. The two lowest frequencies which are $St = 0.05$, and 0.1, turned out to be extreme cases where the flow field was much more developed to the right side of the channel. This phenomenon was directly linked to the fact that the first jet swing is to the right, which triggered an imbalance that would be amplified during every next oscillation, at such low frequencies. As the frequency was increased, this effect gradually disappeared with an increasing average stagnation Nu, since vortices had more coherent structures for higher frequencies; up to $St = 0.4$ where the average Nu_0 was the highest, showing a 2.2% improvement over the steady jet case. As of $St = 0.5$ the average Nu_0 started decreasing, because the oscillation period became too short for a vortex to be strong enough to reach the wall. In this study, vortices were found to be very effective flow structures when it comes to heat removal. Whenever, a vortex was present in the proximity of a given span-wise location, Nusselt number would peak there. Propagating local Nu peaks could be traced, along with their corresponding crawling vortices, especially for $St = 0.2$. This was in good agreement with the findings of Chiriac et al. [5]. Data corresponding to $St = 0.05$ and 0.1, were excluded from the comparison conducted in Table 1 since they presented extreme cases in which the flow is asymmetric. However, they were presented to illustrate the effect that led to asymmetric flow fields for greater values of St.

Table 1. Comparison of the average Nu_0

St	*Nu_0*
steady	10.09
0.2	8.54
0.3	9.96
0.4	10.31
0.5	10.30
0.6	10.15
0.75	9.77

REFERENCES

[1].   Ebrahim, M., Silva, L., Ortega, A., Heat transfer due to the impingement of an axisymmetric synthetic jet emanating from a circular orifice: A numerical investigation of a canonical geometry, Proceedings of the International Technical Conference and Exhibition on Packaging and Integration of Electronic and Photonic Microsystems (InterPACK2013), 2013, Burlingame, California, USA.

[2].   Marzouk, S., Mhiri, H., El Golli, S., Le Palec, G., Bournot, P., Numerical study of momentum and heat transfer in a pulsed plane laminar jet, International Journal of Heat and Mass Transfer 46 (2003) 4319-4334.

[3].   HeeJoo, P., Kurichi, K., Arun, S.M., Heat transfer from a pulsed laminar impinging jet, International Communication of Heat and Mass Transfer 32 (2008) 1317-1324.

[4].   Kim, D., A Numerical study on heat transfer in laminar pulsed slot jets impinging on a surface, World Academy of Science, Engineering and Technology, 6 2012-09-20.

[5].   Chiriac, V.A., Ortega, A., A numerical study of the unsteady flow and heat transfer in a transitional confined slot jet impinging on an isothermal surface, International Journal of Heat and Mass Transfer 45 (2002) 1237-1248.

[6].   Camci, C., Herr, F., Forced convection heat transfer enhancement using a self-oscillating impinging planar jet, Journal of Heat Transfer 124 (4) (2002) DOI: 10.1115/1.1471521.